THE ASTROPHYSICAL JOURNAL, 490:863–878, 1997 December 1
© 1997. The American Astronomical Society. All rights reserved. Printed in U.S.A.

DUST AROUND MAIN-SEQUENCE STARS: NATURE OR NURTURE BY THE INTERSTELLAR MEDIUM?

PAWEL ARTYMOWICZ[1,2] AND MARK CLAMPIN[2]
Received 1996 December 3; accepted 1997 July 15

ABSTRACT

Dust from the interstellar medium (ISM) can collide with and destroy particles in the circumstellar dust disks around main-sequence stars (Vega/β Pic stars). Two current theories tying the occurrence of the Vega/β Pic phenomenon to the erosive influence of the ISM are critically reconsidered here. Using the local standard of rest frame, we find little evidence for a correlated motion (streaming) of prominent disk systems, which one theory suggests would result from a passage about 10^7 yr ago of these stars, but not the control A-type stars, through the nearby Lupus-Centaurus interstellar cloud complex. Moreover, the prototype system of β Pic could not have retained dust produced in such a passage for much longer than 10^4 yr. We show theoretically that the ISM sandblasting of disks has minor importance for the structure and evolution of circumstellar disks, except perhaps in their outskirts (usually >400 AU from the stars), where under favorable conditions it may cause asymmetries in observed brightness and color. The ISM neither produces the disks (as in one theory) nor depletes and eliminates them with time (as in another theory), because typical ISM grains are subject to strong radiative repulsion from A- and F-type dwarfs (a few to 100 times stronger than gravity). Atypically large ISM grains are not repelled strongly, but are unimportant on account of their small number density.

Dust production and destruction in β Pic-type disks results mainly from their collisional nature enhanced by the radiatively produced eccentricities of particle orbits, rather than from nurture in a hostile ISM. The residence times of the few-micron dust grains predominant in the densest part of the β Pic disk is only 10^4 yr, or a few dozen orbital periods. Submicronic debris is blown out as β meteoroids, carrying away from this system an equivalent of the solar system's total mass in solids (~ 120 Earth masses) in only ~ 65 Myr. This rate of collisional erosion exceeds almost 10^8 times that of the zodiacal light disk of our own system. A massive and relatively young ($\lesssim 10^2$ Myr) planetesimal disk appears to surround β Pic, destined to decline in dust density over time comparable to its age. Other dust disks, like those around Fomalhaut and Vega, contain much less dust and may be much older than the β Pic disk, but like the β Pic disk they are also derived from and replenished many times during their lifetimes by unseen parent bodies.

Subject headings: accretion, accretion disks — circumstellar matter — dust, extinction — solar system: formation

1. INTRODUCTION: THE VEGA/β PIC PHENOMENON

As revealed by the multiwavelength (near-infrared to millimeter) observations of radiation thermally emitted by the cold circumstellar matter (typical temperatures $T \sim 10^2$ K), β Pictoris, Vega, Fomalhaut, and other main-sequence stars of their class are known to be surrounded by solid grains in orbit around the stars. According to Patten & Willson (1991), Aumann & Good (1990), and Backman & Paresce (1993), between 10% and 50% of the main-sequence dwarfs of types A to G exhibit the Vega phenomenon, defined as a substantial excess of infrared (IR) radiation over the photospheric flux, emitted by the solid grains accompanying the star with no apparent or suspected mass loss.

Although Vega (α Lyr) was historically the first star to exhibit the telltale IR excess in *IRAS* satellite observations (Aumann et al. 1984), the southern star β Pictoris (β Pic) soon became the leading example of the Vega phenomenon, not only because of its large bolometric excess, equal to 2.4×10^{-3} of the stellar flux, much larger than Vega's excess of 1.5×10^{-5} times the stellar flux, but chiefly because β Pic was the first object to show clear evidence of a thin disk structure. Resembling the solar system's zodiacal cloud and/or Kuiper belt, the disk was imaged coronographically in the visible and near-IR stellar scattered light by Smith & Terrile (1984) and other teams (e.g., Paresce & Burrows 1987; Lecavelier et al. 1993; Golimowski, Durrance, & Clampin 1993; Kalas & Jewitt 1995). The optically and geometrically thin disk extends to large distances ($\sim 10^3$ AU) from the star. The bright dust grains (visible albedo $\gtrsim 0.4$), scattering without significant color effects, with size spectrum peaking near the radiative blowout limit of ~ 1 μm, have an impressive combined surface area, comparable to the area of the heliocentric orbit of Uranus (Artymowicz, Burrows, & Paresce 1989; Burrows et al. 1995). Particles smaller than ~ 5 mm have a total mass on the order of 1 Earth mass (Zuckerman & Becklin 1993). There is strong spectroscopic evidence for planetesimal-sized bodies (comets) evaporating during passage in the close vicinity of the star (Beust et al. 1994; Beust & Morbidelli 1996). The existence of Moon-sized objects (Paresce & Artymowicz 1989) and larger, planet-sized bodies has been postulated. The latter could assist in the creation of the central disk gap (Smith & Terrile 1984; Roques et al. 1994; Sicardy 1994; Burrows et al. 1995) and the moderate-to-large asymmetries thought to be present in both the vertical and the azimuthal distribution of dust in the disk (see

[1] Stockholm Observatory, S-133 36 Saltsjöbaden, Sweden; pawel@astro.su.se.
[2] Space Telescope Science Institute, 3700 San Martin Drive, Baltimore, MD 21218; clampin@stsci.edu.

Lagage & Pantin 1994, Kalas & Jewitt 1995, and Burrows et al. 1995 for observations; Roques et al. 1994, Lazzaro et al. 1994, and Artymowicz 1994b for theories). The total mass of the unseen large bodies is still poorly known.

In the prevailing view, β Pic and other members of its class are evolving young planetary systems currently undergoing a more or less rapid (depending on density of solids) collisional grinding and/or gravitational clearing epoch. This stage of evolution is thought to last between 10^8 and 10^9 yr, following a shorter ($<10^7$ yr) formative era, during which a pre–main-sequence star is surrounded by a relatively massive gaseous protostellar/protoplanetary disk (and during which, by definition, it is not a Vega-type star).[3] It is possible that with time the Vega phenomenon of any particular object (i.e., IR excess, amount of dust, spectroscopic signatures) subsides to a level currently undetectable.

For relevant information about Vega/β Pic-type systems that cannot be summarized here, the reader is strongly encouraged to consult the reviews of the Vega phenomenon and individual objects by Walker & Wolstencroft (1988), Norman & Paresce (1989), Backman & Paresce (1993), Lagrange (1995), Artymowicz (1994a, 1996, 1997), Vidal-Madjar, Lecavelier, & Ferlet (1997), and references therein.

Vega-type objects, except those (most likely post–T Tauri) systems that still retain their massive gaseous disks (Artymowicz 1996), vary considerably in "dustiness," the dust-covering factor $\tau_{\rm dust}$, between $\tau_{\rm dust} = L_{\rm IR}/L_* \sim 10^{-6}$ and $\sim 10^{-3}$, the largest value belonging to β Pic. Here, $L_{\rm IR}$ denotes the total IR excess, and L_* the bolometric stellar flux.

Properties of the dust grains also vary considerably. Does this reflect mainly the age and evolutionary stage of each system, differences in the initial conditions of the disks connected with star formation, or perhaps the influence of the Galactic environment? It is important to know whether internal or the external factors control the evolution of Vega-type systems. In the first case, the Vega/β Pic phenomenon would be a matter of nature, rather than nurture, and the observed state of a given system could, at least in principle, be used to infer its past history. The quantity and the properties of the dust in different objects could then be understood in terms of different stellar masses and luminosities, and different age and initial conditions for the disk. In the latter case, even assuming a perfect knowledge of planetary system evolution, the status and history of each system and the relations between the various main-sequence IR-excess stars would be much more difficult to understand. This is because the strength and even the existence of the IR excess and other observable signatures would in that case depend mainly on environmental factors such as the density, number flux, and energy flux of the local interstellar medium (ISM) through which the star is now or recently was traveling. Two theories highlighting the possible role of the ISM in the evolution of Vega-type systems have recently been formulated (see Backman & Paresce 1993 for a review).

Lissauer & Griffith (1989; hereafter LG) proposed that "sandblasting" by interstellar dust can be a dominant mechanism in the evolution of circumstellar particulate disks. They noticed that stars spend a few percent of their main-sequence life crossing atomic gas clouds, and estimated that circumstellar disks may be eroded significantly during such encounters, especially if the relative encounter velocity is large ($v \gtrsim 10$ km s^{-1}; the rate of erosion is proportional to v^3). β Pic, which has the largest grain population among the Vega stars with resolved disk structures discussed by LG, happens to have an anomalously small average velocity with respect to the local standard of rest, equal to $v_* = 3$ km s^{-1}. The other nearby A-type stars have an average velocity of $v_* = 16^{+12}_{-7}$ km s^{-1}. This led to the proposal that the prominence of β Pic among the resolved examples of the Vega phenomenon is due to a lack of erosion in the hostile ISM rather than to young age or other internal factors.

A different perspective on the role of ISM in the history of particle disks was offered by Whitmire, Matese, & Whitman (1992; hereafter WMW). These authors have argued that the spatial motion of a group of five prominent nearby A-type Vega stars is tightly correlated, and that their mean velocity vector (velocity centroid) points away from one of the nearest major interstellar cloud complexes in Centaurus (the Sco-Cen, a.k.a. Lupus-Centaurus, at a somewhat poorly known distance of 100–200 pc). According to the authors, these stars passed through the dense ISM region 5 to 10 Myr ago. They propose that from among many A-type stars harboring particulate disks, those that were recently subject to ISM "sandblasting" became especially prominent examples of the Vega phenomenon as a result of the fragmentation of circumstellar meteoroids by the ISM. The stars not exhibiting IR excess, on the other hand, could harbor numerous but inconspicuous meteoroids comprising an insignificant combined area.

These two theories appear to give mutually incompatible explanations for the large dust area around β Pic and the (currently) spatially unresolved Vega stars, the first suggesting that β Pic was spared the ISM sandblasting at all times, while the other maintains that, on the contrary, it was recently subject to an intense erosion. Which view is more plausible?

In the present paper we reconsider the interaction of the ISM with β Pic-type stars and find that neither of the current theories is satisfactory. We find that: (1) the two-dimensional motion of the Vega-type stars considered by WMW is uncorrelated (they do not stream together) when viewed in the frame of the local standard of rest. The number of Vega-type stars that passed close to the Lup-Cen stellar association within the past ~ 10 Myr (see § 2) is the same or smaller than the corresponding number from a control group of A-type stars. (2) Sandblasting by the ISM is not effective, because the ISM dust is strongly repelled by radiation pressure from A-type stars (see § 3). (3) "Internal sandblasting" within disks similar to β Pic is a few orders of magnitude stronger than the typical ISM counterpart (see § 4). We thus ascribe the Vega phenomenon to the nature of normal stars, rather than to nurture in a hostile ISM environment. However, weak external sandblasting can, in principle, leave an imprint on the outermost tenuous regions of the disks, which the typical ISM grains can reach. We evaluate such effects and compare them with the internal sandblasting in § 5.

2. ON THE KINEMATICS OF VEGA STARS

Both WMW and LG considered nearby A-type stars from the Gliese catalog for which Galactic coordinates and

[3] Vega-type stars are not, as a rule, associated with or even near to any region of ongoing star formation. In fact, many of the $>10^2$ stars with substantial IR excess have ages from 1 to 5 Gyr (Backman & Paresce 1993).

velocities are available. Using van Altena, Lee, & Hoffleit (1995) as a source of spatial information and Gliese (1969) as a source of kinematical information, we have reconsidered the spatial motion of the WMW star sample (partially overlapping with that of LG) in the physically most appropriate system of reference, i.e., the local standard of rest (LSR). While velocity dispersion will be the same in other reference frames (heliocentric, Lup-Cen), we must compare velocity dispersions with centroid velocity components that do depend on the frame of reference. Note, for instance, that WMW worked in the Lup-Cen reference frame, which happens to move relatively fast with respect to the LSR, thus creating an illusion of streaming for any set of objects that, like a subset of the Vega-type stars, move sufficiently slowly with respect to the LSR. The suspected streaming would require that the centroid velocity in the LSR be larger than the dispersion along each axis.

In Table 1 we present the Galactic coordinates (X, Y, Z) and the corresponding velocities [U, V, W, and $v_* = (U^2 + V^2 + W^2)^{1/2}$] of WMW's set of nearby A-type stars in the standard coordinate system, with the X axis pointing away from the Galactic center (i.e., toward $l = 180°$), the Y axis pointing in the direction of motion of the LSR ($l = 90°$), and the Z axis pointing toward the north Galactic pole. (Notice the opposite orientation of the X axis in WMW). Positions were calculated from the geometric parallaxes and Galactic coordinates of the objects. According to Mihalas & Binney (1981), the Sun's velocity vector in the LSR frame is (−9, 12, 7) km s^{-1}, with a small uncertainty, on the order of 1 km s^{-1}. This velocity was used to convert the motion of stars from the heliocentric to the LSR frame. The Lup-Cen cloud is a complicated object with a poorly known distance of between 100 and 200 pc. We adopted the distance of 125 pc and Galactic coordinates $l = 320°$ and $b = 15°$ for the center of the Lup-Cen association. We note that this distance is likely an underestimate favoring the WMW hypothesis. As did WMW, we assume that its velocity can be approximated by the known velocity of a stellar Lup-Cen association (Eggen 1983; see entry 24 in our Table 1).

Comparison with the results of WMW and LG shows good agreement between the centroid motions (mean velocity) and velocity dispersions of the two groups of stars considered here, and also between individual velocities of stars with respect to the LSR. Particularly worth noting is the fact that β Pic's velocity is the lowest (5 km s^{-1}, cf. 4 km s^{-1} derived by LG).

In contrast to WMW, we find little evidence that the five Vega-type stars (β Pic, α Lyr, α PsA, β Leo, and ζ Lep) have unusual streaming motion in the Galaxy. As a group, they move with velocity ($5 \pm 6, 0.2 \pm 5, -2.2 \pm 0.7$) km s^{-1}. The motion of the centroid in two directions (X and Y) is significantly exceeded by the velocity dispersions, which contradicts the proposed streaming. Only the vertical (Z) motion can be considered correlated, at the 3 σ level. That correlation is responsible for most of the statistical difference first

TABLE 1

GALACTIC COORDINATES AND MOTIONS OF FIVE β PIC-TYPE AND CONTROL A-TYPE STARS

No.	Star	X	Y	Z	U	V	W	v_*
				Sample of Vega-excess stars				
1.....	β Pic	3.3	−16	−10	2	−4	−2	5
2.....	α Lyr	−2.9	7	2.7	8	6	−1	10
3.....	α PsA	−2.7	1	−6	−4	5	−3	7
4.....	β Leo	1.4	−4	13	15	−7	−3	17
5.....	ζ Lep	16	−13	−7.9	5	1	−2	6
	Mean	3	−5	−1.7	5.2	0.2	−2.2	9
	Dispersion	7	9	8	6	5	0.7	4
				Nearby A-type stars				
6.....	κ Phe	−3.8	−3.4	−16	−3	8	−5	10
7.....	β Ari	10	8	−11	−7	1	4.0	8
8.....	τ^3 Eri	9	−6	−18	−25	21	8	34
9.....	1α CMa	1.8	−1.9	−0.4	−24	12	−4	27
10.....	α Pic	−0.5	−16	−7	13	−8	−2	15
11.....	α Gem	13	−1.7	6	−2	8	−4	9
12.....	δ Vel	−0.7	−20	−2.6	−16	11	4	20
13.....	ι UMa	12	1.7	11	23	−2	−8	24
14.....	α Vol	−4.3	−19	−4.5	−17	10	0	20
15.....	δ UMa	7	7	16	−21	12	−2	24
16.....	ι Cen	−10	−12	8	15	−10	3	18
17.....	α^2 Lib	−15	−5	12	2	5	1	6
18.....	β Cir	−17	−13	−0.4	−5	−7	−1	9
19.....	η Oph	−20	2.4	5	−6	21	9	24
20.....	44 Oph	−21	0.6	2.2	27	1	−3	27
21.....	α Aql	−3.4	3.7	−0.8	20	2	5	21
22.....	α Cep	2.9	15	2.5	0	1	0	1
	Mean	−2.4	−3.6	0	−1.5	5	0.3	17
	Dispersion	12	10	9	17	10	5	12
				Other objects				
23.....	Sun	0	0	0	−9	12	7	17
24.....	Lup-Cen	−93	−78	32	−3	−13	−1	13

NOTE.—Positions are given in pc, velocities in km s^{-1}. For Gliese catalogue numbers of objects, see WMW.

noticed by WMW between the five Vega stars and the control group. The origin of the systematic (negative) vertical velocity is unclear. It may be physical, or merely the result of small-number statistics. However, a one-dimensional correlation is not sufficient to establish the fact of streaming required by the WMW hypothesis. For the control stars, all of the centroid velocity components are much smaller than the dispersions: -1.5 ± 17, 5 ± 10, and 0.3 ± 5 km s^{-1}. This is natural, since in the limit of a large sample, the centroid of A-type dwarfs moves at only a few km s^{-1} with respect to the LSR. The dispersions of the control stars are close to those of A-type dwarfs (Mihalas & Binney 1981; Westin 1985). On the other hand, the five selected Vega stars have about two times smaller dispersions, as first shown by WMW. This could be due to the young age of these stars as compared to the general sample (at most on the order of 100 Myr, whereas the main-sequence lifetimes of Fomalhaut and Vega, for example, are 700 Myr and 400 Myr, respectively).

Assuming rectilinear motion over the short time span of $\sim 10^7$ yr considered here (to evaluate the WMW model), and using data from Table 1, we can trace back in time the motion of each individual star with respect to the LSR. The XY projections of trajectories so obtained are shown in Figure 1. Centroid motions (discussed by WMW) are shown as squares. Notice that given the large velocity spread, the centroid trajectory is highly uninformative about the real paths and histories of the stars in the sample. All the trajectories emanate from a circle of radius 25 pc

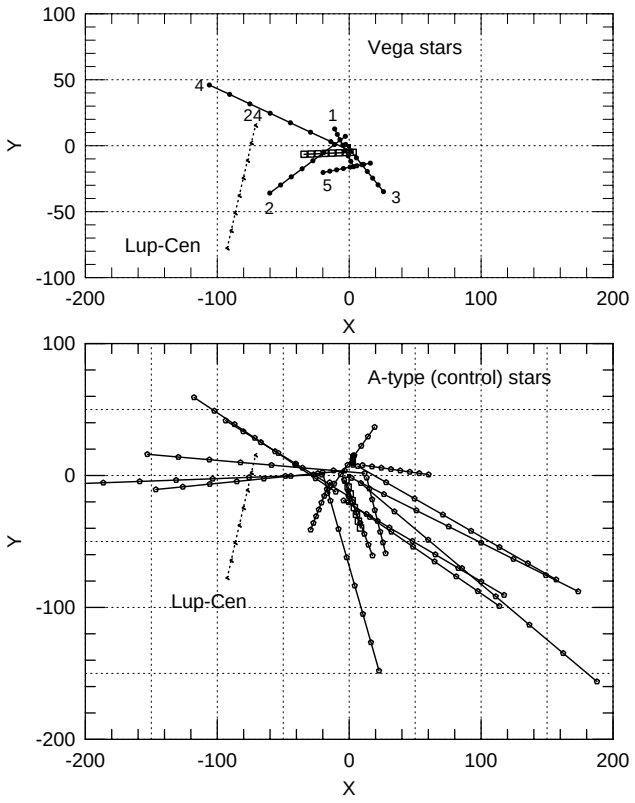

FIG. 1.—The XY projection of motion for five Vega-excess stars (*top*), and 17 control A-type dwarfs (*bottom*). All distances are in pc. Points along the paths are spaced 1 Myr apart in time. Numbers in the top panel are from column 1 of Table 1, and are placed close to the positions of objects 7 Myr ago. Dashed lines show the motion of the Lup-Cen stellar association, representative of the motion of the dense ISM in that region. Squares denote the centroid positions of Vega-type (*top*) and control (*bottom*) stars.

surrounding the origin (Sun's position), except the Lup-Cen association, which changes location from the negative to the positive Y axis (≈ 6 Myr ago). The relatively larger dispersion of velocities for control stars found by WMW is easy to see by comparing the top and bottom panels. However, both groups of stars simply expand, without evidence of streaming together when traced back in time over the past 10 Myr. We also notice that much of the centroid motion toward the negative X axis hinges on the inclusion in the five-star sample of one star, β Leo, with a less significant IR excess than the other stars (that so perhaps should be given a smaller statistical weight). Removing β Leo from the small sample changes the conclusion significantly; repeating the calculations done by WMW, we would conclude that many dozen Myr rather than ≈ 10 Myr are necessary for the centroid of Vega stars to trace back to the estimated position of the Lupus cloud (which might actually not have existed so long ago).

WMW assumed a certain constant shape of the boundary of the Lup-Cen ISM complex (running at a small angle to the Y axis in their Fig. 3). We reach our conclusions without drawing this rather uncertain boundary shape on our plot. Unlike WMW, we do not strive to predict precisely when the centroid might have crossed an assumed boundary of *constant* shape and orientation (an assumption difficult to defend, given a lifetime of clouds and ISM bubbles similar to the time interval of ~ 10 Myr considered). (As already mentioned, centroid motion in the LSR is not representative of the motion of stars in the sample, and thus is irrelevant even if the motion of the cloud boundary were perfectly known.) Instead, we simply observe that both some Vega-type stars and some control stars were in the general vicinity of the young Lup-Cen association 5–10 Myr ago, and conceivably might have interacted with the ISM of the Sco-Cen complex. It would be a vast overinterpretation to claim, based merely on centroid trajectories and an assumed rigid cloud boundary, that the Vega-type stars passed through that complex and acquired their strong IR excesses, while most of the control stars did not and thus remained inconspicuous. On the contrary, there is evidence, as shown in Figure 1, that 7 Myr ago four control stars were passing through the nearby dense ISM, while only one or two Vega stars could be located there. If passage through dense ISM causes the Vega-type excess, then the control stars from Table 1 should now contain more than five Vega stars instead of none, while some of the five strong Vega-excess stars should show no excess. Moreover, the two most prominent prototype Vega stars, β Pic (No. 1) and α PsA (No. 3), have the smallest chance of a recent encounter with Lup-Cen because of their slow and inappropriately directed velocity vectors (see Fig. 1).

Finally, at least in the case of β Pic, the circumstellar dust generated during passage through a dense cloud many Myr ago would have been depleted back to the lower, preencounter equilibrium density on a short timescale, on the order of $t_{\rm dust} \sim 10^4$ yr (the equilibrium dust destruction and replenishment time, cf. § 4.3 below). The ISM-β Pic encounter would have had to have occurred within several $t_{\rm dust}$ to leave observable dust excess. Given the small velocity of the star ($v_* = 5$ km s^{-1}), the encounter would have to occur at an unreasonably small distance of $\lesssim 0.1$ pc, within the local warm ISM bubble. Thus, the explanation of the Vega phenomenon based on streaming stellar motion and durable effects of ISM-disk encounters appears to be incorrect.

3. INTERSTELLAR DUST AROUND A-TYPE STARS

In this section, we discuss the effects of radiation pressure exerted on the ISM dust. We neglect gas-dust coupling in the ISM. One possible mode of coupling could exist if grains were decelerated by stellar radiation, leaving the ISM gas unaffected, which might result in a back-wind drag force on grains. It can be shown that the maximum such force in a dense atomic cloud (density $\sim 10^{-24}$ g cm^{-3}) is $\sim 10^{-5}$ times weaker than the stellar gravitation or radiation pressure on dust at a point where these two dominant forces are equal. Another process, magnetic coupling between charged ISM grains and gas, likewise does not dominate radiation or gravity, except in an unlikely case where magnetic field energy exceeds both the energy of the outflowing stellar wind and the thermal energy of the incoming ISM gas. Below we discuss the shape of the avoidance zone around a star where dust with given properties cannot enter, and compute its characteristic size for several stars, showing that the ISM is not the agent controlling the evolution of their disks.

3.1. *Radiative Rutherford Scattering of Dust*

While the importance of radiation pressure for the circumstellar dust (e.g., for the lower size cutoff and such) has long been appreciated, stellar radiation pressure on ISM dust is conspicuously absent from existing theories. The repulsive inverse-square force that a typical 0.1 μm ISM grain feels when approaching an A-type star (such as the first five stars in Table 1) is many times larger than gravity ($\beta - 1$ times larger, where β is the ratio of radiation pressure to gravity). This leads to Rutherford scattering of grains off the star (analogous to Rutherford scattering of positively charged particles off atomic nuclei). Let v_∞ be the velocity of a grain infinitely far from the star in the inertial system attached to a star of mass M. From energy conservation, the grain cannot approach the star closer than its avoidance radius, $r_{\rm av}$, given by

$$r_{\rm av} = \frac{2(\beta - 1)GM}{v_\infty^2} . \tag{1}$$

If we adopt v_∞ as the unit of velocity, the avoidance radius as the unit of distance, and $r_{\rm av}/v_\infty$ as the unit of time, then the equation of motion for the nondimensional vector $\boldsymbol{R} = \boldsymbol{r}/r_{\rm av}$ reads

$$d^2\boldsymbol{R}/dt^2 = \boldsymbol{R}/(2R^3) . \tag{2}$$

Several dozen solutions of this equation, simulating a uniform density line or stream of particles approaching a star from infinity ($x = +\infty$) with the same initial velocity $\boldsymbol{v} = (-v_\infty, 0, 0)$ are overplotted in Figure 2. Positions of the particles plotted as open circles are uniformly spaced in time. While some grains undergo large-angle backscattering, most are gently deflected, so that an empty parabolic wake bounded by a high-density wall is evacuated. A star moving through a three-dimensional cloud of grains with constant β will be surrounded by an axisymmetric paraboloidal void described by the equation $x/r_{\rm av} + [(y/r_{\rm av})^2 + (z/r_{\rm av})^2]/4 = 1$. It is straightforward to demonstrate that if a star has a sufficiently large planar disk inclined by angle θ to the direction of the initial relative velocity $\boldsymbol{v}_\infty$, then the region of avoidance within the disk has an elliptical shape with minimum and maximum distances from the star equal

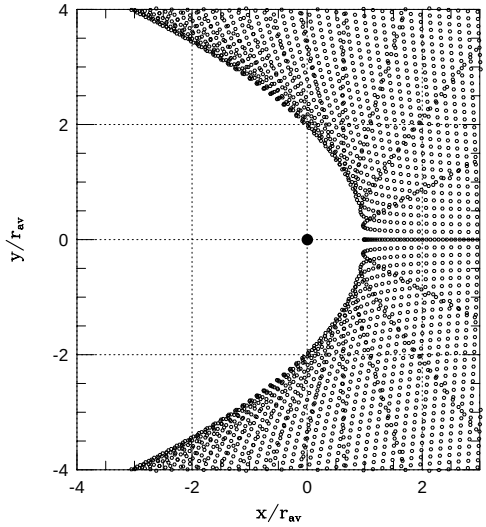

FIG. 2.—Cross section of a cloud of particles (*circles*) with constant radiation pressure parameter $\beta > 1$, approaching the star (*large black dot*) from the right with uniform initial density and velocity. The particle approaching along the X axis comes closest to the star: it turns back by 180° at the distance of one avoidance radius $r_{\rm av}$, as defined by eq. (1). Other particles undergo smaller deflections and remain at larger distances, leaving a large empty paraboloidal wake.

to

$$r_\pm = 2r_{\rm av}\frac{|\cos\theta \mp 1|}{\sin^2\theta} . \tag{3}$$

For example, if $\theta \to 0$, then $r_+ \to r_{\rm av}$ and $r_- \to -\infty$, and the situation depicted in Figure 2 is attained. At an intermediate disk inclination angle $\theta = 45°$, the void around the star intersects the disk along the ellipse at distances from 1.17 to 6.83 times $r_{\rm av}$. If the ISM grains approach along the disk axis of symmetry, at $\theta = 90°$, then the circular avoidance zone has a radius of $r_+ = r_- = 2r_{\rm av}$, or as much as twice the avoidance radius of in-plane bombardment ($\theta \approx 0°$). This can be visualized in Figure 2 by placing the disk in the $x = 0$ plane.

3.2. *Avoidance Radii for the ISM Grains around A-type Stars*

Using Mie theory as in Artymowicz (1988), we have computed β as a function of grain radius s for composite silicate-carbonaceous particles modeling the ISM grains (Mathis 1996). The new features implemented in our code include the addition of a mantle (third material) to the two core materials considered before (core = matrix + interspersed inclusions). We used the Maxwell-Garnett effective medium theory (Bohren & Huffman 1983) first to compute the effective dielectric constant of the grain's core at each wavelength, and then to combine it with the appropriate constant for the mantle.

We use the complex refractive indices of Draine & Lee (1984) for the "astronomical silicate" (DL silicate) and the carbon material (graphite). We did not simulate icy mantles because water ice (and contaminating ice) is rapidly destroyed by UV photosputtering (cf. Artymowicz 1996). Vacuum was used as a mantle material to simulate porosity of the grain. We have also experimented with real (i.e., laboratory) data replacing the DL dielectric constants. Olivines ($MgFeSiO_4$) and an assortment of other widespread

TABLE 2

AVOIDANCE RADII AND β FOR ISM GRAINS AROUND THREE STARS

Star	β Pic	α PsA	α Lyr
Spectral type.....	A5	A2	A0
L/M	5	6.5	24
v_∞ (km s^{-1}).....	8.6	9.9	12.2
$r_{\rm disk}$ (AU).....	60	$\sim 10^2$	~ 90
Porous silicate + graphite grains			
$\beta(s \to 0)$.....	12.8	18.2	81
$\beta_{\rm max}$	19.2	27.0	111
$s(\beta = 1)$ (μm).....	2.9	3.6	12
r_0 (AU)	500	595	2780
$r_{0.1}$ (AU)	765	895	3530
Compact silicate + graphite grains			
$\beta_{\rm max}$	24.8	34.8	130
$s(\beta = 1)$ (μm).....	1.6	1.95	6.3
$r_{0.1}$ (AU)	940	1060	3630

silicate minerals and rocks (basalt, iron-rich pyroxenes) produce results similar to those presented below. Recently, Mathis (1996) modeled ISM grains based on interstellar extinction and new metal abundance constraints. The model grains consist of oxides, silicates, various carbon forms (either intermixed or separate from silicates), and vacuum, in proportions that are determined by fits to observations. The preferred model is a composite consisting of (roughly) equal amounts of carbon and silicates, with minor amounts of additional pure silicates and graphite, and favors nonextreme porosity (45% of vacuum; in any case the porosity is $<80\%$, Wolff, Clayton, & Meade 1993). We shall consider grains combining equal volumes of DL silicate and graphite, and 0% or 50% of vacuum. Following from bulk densities of graphite and silicates,[4] the two grain models have mean densities of 1.12 and 2.23 g cm^{-3}, respectively.

We consider the three best-studied Vega-type stars: β Pic (A5 V), α PsA (Fomalhaut, A2 V), and α Lyr (Vega, A0 V). These three examples span a sufficient range of luminosity-to-mass ratios to illustrate the effects of different stellar characteristics on ISM grain repulsion, and to provide the basis for rough extrapolation to F V stars. Observed UV stellar fluxes must be used to represent the spectra of the stars, or else large errors in β might occur for small grain sizes (up to 20% when the blackbody spectrum is used). We have compiled spectra covering wavelengths from 0.2 μm to 150 μm using the *IUE* fluxes (recalibrated by R. Bohlin; 1995, private communication) augmented in the far-UV and at $\lambda \gtrsim 3300$ Å with the Kurucz's model atmosphere fluxes. Parameters for the β Pic, α PsA, and α Lyr photospheric models, respectively, are $T_{\rm eff} = 8000$ K, $\log g = 4.0$; $T_{\rm eff} = 8800$ K, $\log g = 3.5$; and $T_{\rm eff} = 9400$ K, $\log g = 3.95$. Furthermore, we adopt the bolometric luminosity-to-mass ratios $L/M = (L/L_\odot)(M_\odot/M)$ given in Table 2. These values are in agreement with the mass-luminosity relations and the bolometric luminosities determined from trigonometric parallaxes. The recently revised luminosity of β Pic, equal to 8.7 $L_\odot$ (Crifo et al. 1997), leads to $L/M = 5$ (assuming $M = 1.75\ M_\odot$), as compared to an earlier estimate of $L/M = 4$ (e.g., Backman & Paresce 1993), making the radiation pressure 25% stronger than previously thought.

We substitute L/M values into the formula for the ratio of radiation pressure to gravity (Burns, Lamy, & Soter 1979),

$$\beta = 0.57 Q_{\rm pr} (L/M)(s/\mu{\rm m})^{-1}(\rho/{\rm g\ cm^{-3}})^{-1}\ , \qquad (4)$$

where s denotes particle radius, ρ is the bulk density of grain material, and $Q_{\rm pr}$ is the radiation pressure efficiency averaged over the stellar spectrum (the result of Mie theory calculations, tending to unity for grains with $s \gg 1$ μm).

Figure 3 shows the log-log plot of the radiation pressure coefficients of porous and compact grains subject to illumination by three A-type stars. We believe that the porous-grain model is more realistic, but display results for nonporous grains for comparison. Like other authors (e.g., Wolff et al. 1994), we find that porosity moderates the peak values of β, broadening and shifting the peak toward larger grain radii. The large values we obtained are mainly due to the carbonaceous, highly absorbing nature of the ISM grains, which strongly couple to blue stellar radiation. In Table 2, we quote two characteristic values of β, the asymptotic value for small grains, $\beta(s \to 0)$, and the maximum value, $\beta_{\rm max}$, achieved for grains with radius on the order of 0.1 μm. The asymptotic values (and hence avoidance radii) for porous and compact grains are equal. We see that $\beta(s \to 0) \sim \beta_{\rm max} \gg 1$. The β coefficient decreases for $s \gtrsim 0.1$ μm and reaches unity at $s(\beta = 1) \sim$ (1–10) μm (as shown in Table 2), a size range populated by very few ISM grains (see below). Most of the ISM is thus strongly affected by radiation, given the likely size distribution of grains in the ISM.

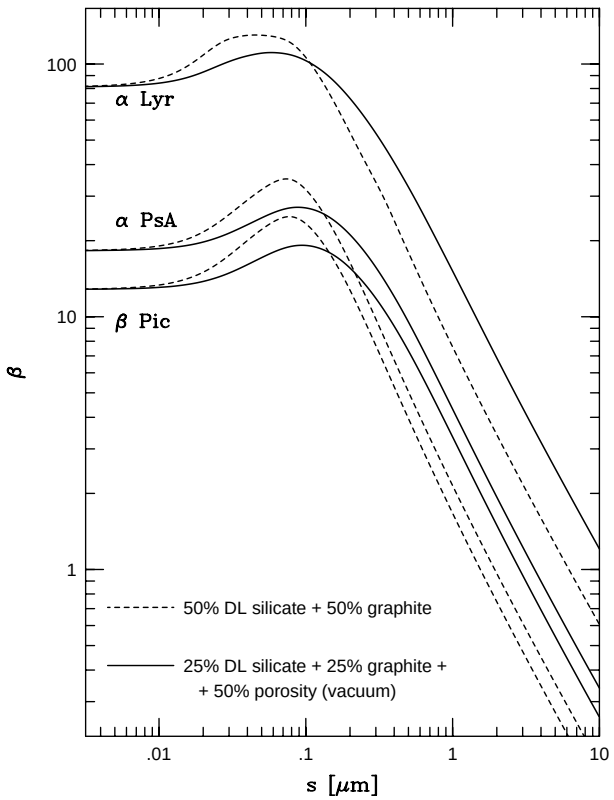

FIG. 3.—Radiation pressure to gravity ratio $\beta(s)$ around three A-type stars for a range of grain radii s and two ISM grain models (porous and nonporous composite silicate-carbonaceous grains)

[4] The DL silicate is assumed to have a density of $\rho = 2.2$ g cm^{-3}, while graphite crystals have a density of $\rho = 2.25$ g cm^{-3}. The last value replaces the incorrect, much higher, value adopted by Artymowicz (1988) after Lamy, Grün, & Perrin (1987).

If a star has a solar wind similar to that present in the heliosphere, its Lorentz force can be of a magnitude similar to that of the radiation pressure (WMW). In this case, magnetic forces provide shielding against the ISM. However, it is well known that normal A-type stars have very little chromospheric and magnetic activity, and are not expected to have a substantial solar wind. No fast outflows, such as would be required to generate substantial Lorentz force and/or strong hydrodynamic drag on grains, are evident in spectra of β Pic. Radiation pressure is probably the only force strong enough to repel and/or deflect ISM grains away from A-type stars.

In order to evaluate avoidance radii, we need to specify the relative star-ISM velocity v_∞. In practice, this important parameter is unknown and may be subject to significant random variations among Vega-type stars. Over a sufficiently long timescale, the average encounter velocity will be given by

$$v_\infty^2 = v_*^2 + v_{\rm ISM}^2 , \tag{5}$$

where v_* is the stellar velocity (cf. the rightmost column of Table 1) and $v_{\rm ISM}$ is the ISM velocity, both reckoned in LSR. Kinematics of gas clouds in the thin Galactic disk requires $v_{\rm ISM} \approx 7$ km s^{-1}, a value about 4 times smaller than the typical velocity dispersion of the stellar disk (e.g., Binney & Tremaine 1987), but not much different from v_* of the Vega-type group. In Table 2 and Figure 4 we present results for the avoidance radii calculated on the assumption that $v_{\rm ISM} \approx 7$ km s^{-1} (and therefore $v_\infty = 8.6$, 9.9, and 12 km s^{-1}) for the three stars considered (Table 2). Based merely on the differences in these v_∞, $r_{\rm av}$ differs by a factor of 2 between α Lyr and β Pic. A larger range of variations of $r_{\rm av}$ could be caused by differing dust-repelling ability, mainly due to different [L/M]. On the other hand, if the vectors of the stellar and ISM velocities are parallel (or antiparallel), then, for instance, in individual encounters of β Pic with standard ISM clouds, v_∞ could equal 2 (or 12) km s^{-1}, deviating from the statistical average of 8.6 km s^{-1} by +3 (or −7) km s^{-1}. Taken together, these uncertainties mean that the computed avoidance radii should be taken as only accurate to within a factor of ~ 2.

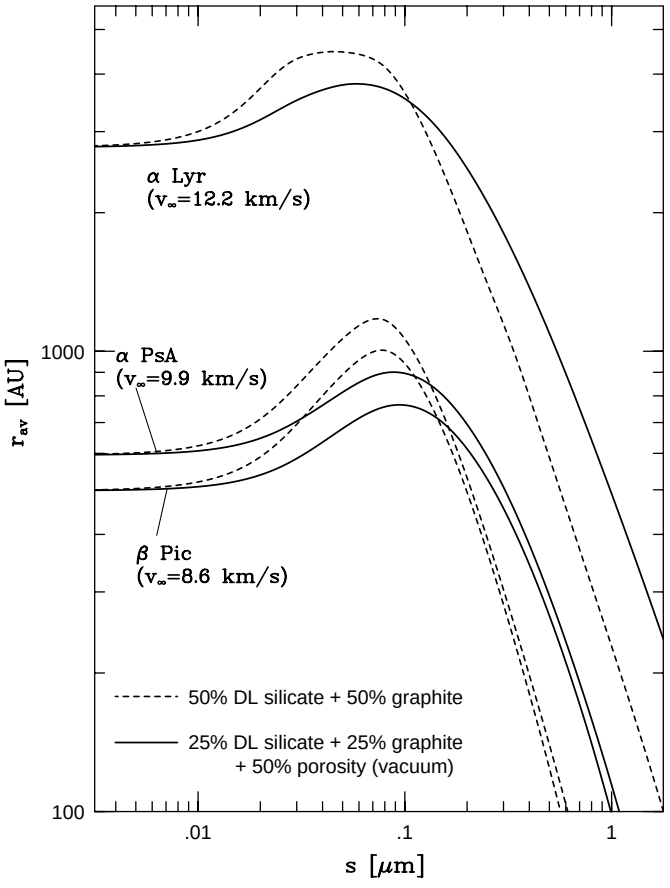

FIG. 4.—Radii of avoidance for ISM grains with properties given in Fig. 3. The three pairs of curves correspond to three A-type stars and their characteristic velocities relative to the ISM (cf. eq. [5]).

The radius r_0 gives the asymptotic value $r_{\rm av}(\beta \to 0)$; $r_{0.1} = r_{\rm av}(\beta = 0.1\ \mu{\rm m})$ is the typical avoidance radius for $s = 0.1\ \mu$m. From Table 2 it follows that $r_{0.1} \gg r_m$ for $r_m =$ 50–100 AU as the maximum circumstellar dust density radius, where most of the thermal IR radiation originates. In other words, submicron-sized grains, which can only approach the star to within one or two avoidance radii (§ 3.1), do not spatially overlap with the dense parts of β Pic-type disks. We shall now argue that virtually all of the ISM falls into this category of strongly repelled particles for which $r_{0.1}$ is the relevant distance of minimum approach.

The mass vs. size distribution of ISM grains (Mathis, Rumpl, & Nordsieck 1977; Kim, Martin, & Hendry 1994; Kim & Martin 1995, 1996; Mathis 1996) peaks in precisely the range $s \sim 0.1\ \mu$m, where A-type stars exert the most radiative effects. For quantitative estimates, we adopt the best-fit analytical formula for the grain size distribution from Mathis (1996) as

$$dN/ds = Ks^{-3.5} \exp\,[-(300s/\mu{\rm m}) - (0.343\ \mu{\rm m}/s) - 50(s/\mu{\rm m})^2] , \tag{6}$$

which represents a standard power law, $dm/ds = K's^{-0.5}$ (K, K' = const), truncated at small ($s \lesssim 0.1\ \mu$m) and large ($s \gtrsim 0.2\ \mu$m) sizes. In contrast, earlier formulations (the so-called MRN law of Mathis et al. 1977) of the form $dm/ds \approx K's^{-0.5} \exp(-5s/\mu{\rm m})$ stressed a sharp upper-end truncation, but allowed for a larger number of small grains. While the existing data do not constrain the low-size end of the distribution well enough to discriminate between the two possibilities (Mathis 1996), we have checked to see that our main results presented in § 5.2 are not affected by this low-mass uncertainty. Most existing formulae for the size distribution of ISM grains, including equation (6), place a negligible number, area, and mass in grains large enough not to be repelled from A-type stars, i.e., larger than $s(\beta = 1)$. Incidentally, such ISM grains would perforce have to be the same size as or larger than normal disk grains, which *are* affected by radiation (and so the process would resemble sandblasting of ISM by disks, not the other way around).

The general conclusion from Table 2, Figure 4, and the ISM size distribution is that quite independent of its spatial concentration, ISM dust is deflected by radiation and remains at distances from A-type stars much larger than the characteristic disk radii. Stars of types F and later exert a weaker radiation pressure (however, $\beta_{\rm max} > 1$ around the Sun), but their stronger magnetized winds may take over the task of maintaining ISM dust–free zones larger than the characteristic disk sizes. It is clear, however, from the best-known example of the β Pic disk that circumstellar disks

may have quite extended outer regions ($r \sim 10^3$ AU) where low disk velocities combined with low spatial densities of dust may allow ISM sandblasting to be important, or even dominant.

4. INTERNAL PROCESSING OF DUST IN DISKS

To assess the possible role of ISM-disk interaction in the outer parts of Vega-type disks, we choose β Pic from among the prominent disk systems as the one (1) least protected from ISM by radiation pressure and (2) sufficiently well-studied to allow quantitative modeling. However, much of the theory applies to other systems as well. In the present section we evaluate the dust destruction rate due to internal erosion, and in the next section we compare it with the ISM sandblasting rate.

4.1. *Distribution and Properties of Dust in the β Pic Disk*

Simultaneous modeling of scattered and reemitted IR radiation has been performed in order to reconstruct the spatial density and composition of disk particles (for a review see Artymowicz 1994a, 1997). One useful model has optical thickness smoothly interpolated between two power laws: an increasing profile inside (in the inner gap region) and a decreasing one outside the characteristic radius r_m near which the optical thickness is maximum [$\tau_m = \tau(r_m)$];

$$\tau(r) = 2\tau_m/[(r/r_m)^{-p} + (r/r_m)^q] , \quad (7)$$

where we adopt $p = q = 2$ ($p = 1$, another possible choice, makes little difference for our purposes here). A value of $q = 1.7$ has often been used in the past, but according to Artymowicz et al. (1989), $q = 1.9 \approx 2$ may be equally appropriate if, as recently observed by Kalas & Jewitt (1995) and Burrows et al. (1995), the disk has an exponential vertical dust area distribution. The radius of maximum dust density, $r_m \approx 60$ AU, follows from its known angular separation (Lagage & Pantin 1994) and the new *HIPPARCOS* parallax for the system, corresponding to β Pic 's distance of 19.3 ± 0.2 pc (Crifo et al. 1997). For comparison, the formerly used distance of 16.4 pc yielded $r_m \approx 50$ AU, making the timescales of internal disk erosion shorter by $\sim 30\%$. In order for the disk dust to intercept the correct percentage of the starlight (reproducing the total IR excess to stellar luminosity ratio of $\tau_{\rm dust} = L_{\rm dust}/L_* = 2.4 \times 10^{-3}$, cf. Backman & Paresce 1993), we require $\tau_m = 4\tau_{\rm dust}/\pi Q_{\rm abs} = 7.64 \times 10^{-3}$, assuming a grain absorptivity $Q_{\rm abs} = 0.4$, both of which values are consistent with observational constraints. (A slightly smaller peak value, $\tau_m = 7.05 \times 10^{-3}$, is obtained in a model with $p = 2$ and $q = 1.7$, which has a relatively larger dust density at large radii).

Dust in the dense part of the β Pic disk is found within a small opening angle of approximately 7° from the disk plane (Artymowicz et al. 1989). To the extent that ISM flow is unlikely to occur at an even smaller angle ($\theta < 7°$) to the disk plane, the detailed manner in which the dust is distributed vertically throughout the disk need not be specified, and the whole disk can be treated as planar (two-dimensional).

We shall make a rough approximation to the actual distribution of particle sizes in the disk by considering spherical "average grains" with radius s_d on the order of several μm, defined by the requirement that there be maximum contribution by grains of radius s_d to the total dust area per logarithmic interval. Appropriate values span the range from $s_d = 2$ μm to $s_d \sim 5$ μm. These grains are required to explain the neutral scattering in the visible spectrum (Paresce & Burrows 1987), inefficient far-IR radiation (e.g., Backman, Gillett, & Witteborn 1992), and the presence and the shape of the 9–12 μm silicate emission feature (which according to Aitken et al. 1993 and Knacke et al. 1993 requires $s \simeq 2$ μm grains at radii $r < 30$ AU, while the main disk may well consist of slightly larger grains). We adopt $s_d = 4$ μm. We have checked using more detailed, multisized disk modeling that monodispersed disk models reproduce the overall internal disk erosion to within a factor of 2, which is the typical accuracy we are aiming for in our present calculation. On the other hand, we will explicitly take into account the ISM size distribution, upon which the avoidance radii and other quantities depend via the $\beta(s)$ dependence.

4.2. *Kinematics and Collisions of Dust in a Disk*

The dominant mechanism of dust evolution in disks is thought to be collisional cratering and catastrophic fragmentation of particles (planetesimals → meteoroids → dust), ending with the radiative removal of submicronic fragments (Artymowicz 1988). The same mass loss per unit time pertains to dust and to larger parent bodies in a stationary cascade. Dust processing in β Pic is qualitatively similar to that occurring in the tenuous meteoritic complex of the solar system (Leinert, Röser, & Buitrago 1983; Grün et al. 1985), but it is quantitatively seven orders of magnitude more intense (cf. below). Velocity dispersion in the disk is much larger than 50 m s^{-1}, an approximate limit to nondestructive encounters. Dust agglomeration is impossible under such conditions, and grain growth from gas is impeded by a gas-to-dust ratio $\ll 1$. Collisions, removing the average grains faster than other processes (most notably the Poynting-Robertson effect), determine the resupply rate and the likely evolutionary timescale for the "clearing" of the whole disk, which with time may transform β Pic's disk into a system more closely resembling our own zodiacal dust disk (or the Kuiper belt). In the standard approach, vertical motions within the disk, leading to the resolved disk thickness, are also held responsible for the frequency of grain collisions (the collision timescale) and the corresponding disk erosion rate (e.g., Backman et al. 1992). However, radiative effects should be even more important (Artymowicz 1997), in the following way.

The observed average grain sizes in Vega-type systems represent a lower cutoff to an otherwise steep power law extending to the larger sizes. They are consistent with the radiative blowout limits, $s(\beta = 1)$, for the respective host stars (cf. Artymowicz 1988 for β Pic; Backman & Paresce 1993). If indeed $s_d \approx s(\beta = 1)$, then $\beta \sim 1$ for the area-dominating disk grains not only in β Pic but also in other systems of its class. The most likely constituent materials, Fe-poor pyroxenes and olivines, exhibit $\beta \approx 0.25$ at the size $s = s_d = 4$ μm. We denote the average disk β as β_d. Such grains are subject to the effective attraction equal to $\frac{3}{4}$ of the gravitational force, and would move at the sub-Keplerian speed of $v_c = (1 - \beta_d)^{1/2} v_{\rm K} = 0.87 v_{\rm K}$ (where $v_{\rm K}^2 = GM/r$) when placed on a circular orbit. Borrowing terminology from solar system studies, we call these observed, orbitally stable particles "α meteoroids."

Consider the creation of average disk particles as fragments of a much larger parent particle, one much less affected by radiation pressure ($\beta \ll 1$). To estimate the

minimum gain of eccentricity by the daughter grain, assume a circular orbit for the parent grain and a velocity of ejection of the debris much smaller than the orbital speed. The initial velocity of the daughter grain is $v_K(r) > v_c$. From energy conservation, it follows that the daughter grain is placed at the periastron of an elliptic orbit with eccentricity $e(\beta) = \beta/(1 - \beta)$. Thus, $\beta = \frac{1}{2}$ suffices for the escape of the debris from the system. This fact is well known in our solar system, where dust from comets and meteoroids can be blown out by radiation pressure at even smaller β (because of parent body eccentricity). The escaping, unbound grains with $\beta > \frac{1}{2}$ are known as β meteoroids. Since grains with a wide range of radii are created in any energetic collision, both stable α particles with $\beta_d < \frac{1}{2}$ and escaping β meteoroids are being produced in large numbers in circumstellar disks. The submicron-sized β meteoroids in the β Pic disk do not contribute much to the optical thickness because of their short residence time, equal to one dynamical timescale. The α particles stay in the system, forming the observed disk. They endow it with significant planar velocity dispersion, corresponding to epicyclic motion with eccentricity $e(\beta_d)$, e.g., $e = \frac{1}{3}$ for our canonical average particles with $\beta_d = \frac{1}{4}$. The full range of eccentricities represented in the disk is, however, very broad ($0 < e < 1$), owing to both a wide range of β and the eccentricities of parent body orbits. On the other hand, inclinations are unaffected by radiation force and are simply inherited from parent bodies, with little addition from the ejection velocities of debris.

Inside the disk, the three-dimensional velocity dispersion can be approximated as $\sigma \simeq ev_c = \beta_d/(1 - \beta_d)^{1/2} v_K$ (i.e., 0.29 v_K for $\beta_d = \frac{1}{4}$). The cross-sectional area for disk-disk particle collision is $4\pi s_d^2$, four times that of particle's cross-sectional area. Several heuristic derivations of the mean collisional lifetime of average grains in disks affected by radiation pressure can be given.

In one approach (Artymowicz 1997), passages of typical grains through the disk are considered to lead to collisions with identical particles with a probability of $4\tau(1 + \sigma^2/\sigma_z^2)^{1/2}$ per orbital period P. Here, σ_z is the vertical velocity dispersion, equal to $iv_c \approx 0.12v_c$, assuming a constant half-opening angle $i = 7°$ of the disk. For a typical particle, as opposed to one with maximum inclination, one full period rather than $P/2$ is needed to vertically cross the full vertical optical thickness τ. The square root factor, in turn, corrects for the effectively larger optical thickness encountered along an eccentric orbit as compared to a circular (inclined) one. The factor σ/σ_z is equal to the ratio of e to i, and the whole correction factor is close to 3. Finally, we obtain

$$t_{\rm coll} \simeq \frac{P}{12\tau} , \tag{8}$$

where $P = 0.77(r/\mathrm{AU})^{3/2}$ yr and τ is given by equation (7).

Alternatively, one can compute $t_{\rm coll}$ from kinetic theory, without reference to orbits. The rate of disappearance of disk particles considered as projectiles reads

$$\dot{n} = 4\pi s_d^2 n^2 \sigma , \tag{9}$$

where n is the local number density of disk particles. Noticing that $\pi n s_d^2 = dr/dz$, the (vertical) spatial derivative of optical thickness, and that $d\tau/dz \approx \tau/(2h)$, where h is the disk's effective half-thickness ($h/r \approx 0.12$, assuming a constant 7° half-opening angle of the disk), we can write the alternative expression for the collisional timescale as

$$t_c = n/\dot{n} = h(2\tau\sigma)^{-1} . \tag{10}$$

Substituting for σ and denoting the Keplerian period as P, we obtain

$$t_c = \frac{h}{r} \frac{\sqrt{1 - \beta_d}}{4\pi\beta_d} \frac{P}{\tau} , \tag{11}$$

which evaluates to $t_c = P/(30\tau)$, a result 2.5 times smaller than $t_{\rm coll}$ from equation (8).

At a higher approximation level, reductions in the efficiency of dust destruction need to be taken into account. For instance, in any realistic calculation, a distinction between disruptive nearly head-on collisions and the barely touching oblique strikes must be made, since only the former usually result in ejection from the system of the whole mass of the two colliding bodies in the form of β meteoroids. On the other hand, the dust avalanche process (Artymowicz 1996, 1997) causes a moderate increase of disk erosion in β Pic (but not in the less dusty disks). However, even without including the full range of details, equation (8) reproduces the more detailed, multisize distribution calculations, which are beyond the scope of this paper, to within a factor of 2, while equation (11) gives a somewhat worse agreement. Hence, we adopt equation (8) in the following discussion.

4.3. *Dust Depletion Timescales*

The picture of vigorous planar epicyclic motions within a thin disk yields substantially shorter dust destruction/resupply times than considered earlier. New observations (Lagage & Pantin 1994; Burrows et al. 1995) have confirmed the general correctness of the dust distribution model of equation (7) based on earlier analyses (e.g., model [7] of Artymowicz et al. 1989). Taken together, these theoretical and observational advances allow a relatively accurate (to within a factor of ~ 2) estimation of the overall rate of internal disk erosion, $\dot{M}_{\rm dsk}$, equal to the dust destruction rate

$$\dot{M}_{\rm dust} = 2 \int \frac{dM}{t_{\rm coll}} \simeq \frac{16\pi\rho s_d}{3} \int \frac{\tau(r) r\, dr}{t_{\rm coll}} , \tag{12}$$

where ρ is the bulk density of disk grains, dM is the mass of the disk element treated as target, and the front factor 2 stands for two colliding particles turned into (spherical) β meteoroids. Using equations (7), (8), and (12), we obtain for β Pic $\dot{M}_{\rm dsk} = \dot{M}_{\rm dust} = 1.9 \times 10^{-6} M_{\rm E}$ yr^{-1} (Earth masses per year). The rate of solid-particle grinding at all levels of a steady-state size distribution must thus be close to 4×10^{14} g s^{-1}, a factor of 4×10^7 times larger than in the meteoritic and zodiacal light complex of our solar system ($\sim 10^7$ g s^{-1}, cf. Leinert et al. 1983; Grün et al. 1985).

We discuss several global timescales of interest. First, we express the characteristic dust mass in the disk as $M_{\rm dust} = \int dM = (8\pi\rho s_d/3) \int \tau r\, dr$ (dust area times the mass-to-area fraction for area-dominating grains). In β Pic we have $M_{\rm dust} \approx 0.02\, M_{\rm E}$. Next, we define the average dust residence timescale as

$$t_{\rm dust} = \frac{M_{\rm dust}}{\dot{M}_{\rm dust}} = \frac{\int \tau r\, dr}{2 \int t_{\rm coll}^{-1} \tau r\, dr} . \tag{13}$$

The dust residence (and replenishment) time is independent of s_d, and to within a numerical factor on the order of

several it equals $t_{\rm coll}(r_m)$, the collisional timescale in the region where both τ and τr are nearly maximum. In β Pic, the mean dust residence time following from the above definition is $t_{\rm dust} \approx 10^4$ yr. This is because at $r = r_m \approx 60$ AU the dust survives for only $t_{\rm coll}(r_m) \approx 4 \times 10^3$ yr. The fact that $t_{\rm dust}$ is 10^4 times shorter than the age of the system ($\sim 10^8$ yr; cf. Crifo et al. 1997) means that the observed dust must have been continuously replenished (at least 10^4 times!), unless the disk is a temporary phenomenon decaying on a timescale of 10^4 yr or just tens of orbital periods. (However, dust disks cannot be short-lived in general, because the Vega phenomenon is widespread.) In this way, we arrive at an important conclusion that a very large reservoir of mass, $\sim 10^4 M_{\rm dust} \sim 100 M_{\rm E}$, would be needed to sustain the current dust processing rate in β Pic for its age of $\sim 10^8$ yr. An even larger mass is required if the dust area declines with time. The initial disk mass must be on the order of a whole solar system's mass of solids. Alternatively, constraints on the system's age can be obtained.

One can define the instantaneous disk depletion timescale as $t_{\rm depl} = M_{\rm dsk}/\dot{M}_{\rm dsk}$, where $M_{\rm dsk}$ is the total mass of all solids in the disk. This latter quantity is presently unknown, and can only be estimated theoretically. Planetary systems similar to and including our own are expected to contain, to within a factor of a few, the fiducial mass $M_{120} = 120 M_{\rm E}$ of solids, mainly silicates and ices (cf. Artymowicz 1997). The depletion timescale of a fiducial planetary system,

$$t_{\rm dd} = M_{120}/\dot{M}_{\rm dsk}\ , \tag{14}$$

can be readily calculated using equation (12). In β Pic, $t_{\rm dd} \sim 65$ Myr. This short timescale is marginally consistent with the system's estimated age of $\lesssim 200$ Myr (Paresce 1991; Crifo et al. 1997). The rate of collisional grinding of the β Pic disk appears to be so fast as to require a downward revision of the age to $\lesssim 100$ Myr, unless we are prepared to accept that either the β Pic disk became dusty 10^4 yr ago, or the initial disk mass was much larger than M_{120}, both unattractive propositions.

The large dust destruction rate in our estimates may represent the maximum achievable rate for β Pic's disk geometry and dustiness (Artymowicz 1996, 1997). Systems other than β Pic evolve collisionally on much longer timescales, because of their lower dustiness. For these systems, $\dot{M}_{\rm dsk}$ and $t_{\rm dd}^{-1}$ scale quadratically with the normal optical thickness τ (i.e., τ_m) and the "dust covering factor" $L_{\rm IR}/L_*$, while $t_{\rm dust}$ scales with the inverse of the optical thickness. For instance, if the spatial distribution of dust around α PsA and α Lyr were similar to that around β Pic, except for normalization, then following from the known dust-covering factors (2.4×10^{-3} for β Pic, 5×10^{-5} for α PsA, and 1.6×10^{-5} for α Lyr), their collisional dust depletion/replenishment times would both still be relatively short, $t_{\rm dust} \sim 0.1$–1 Myr, while the collisional depletion of a planetary system would take an extremely long time, $t_{\rm dd} \sim 120$ Gyr for α PsA and almost ten times longer for Vega. (Cf. $t_{\rm dd} = 214$ Gyr in one detailed model of α PsA, recorded as No. 9 in Table 3.) This does not imply that normal Vega-type stars all have low-mass disks and true planetary systems, but only that their possible planetary systems are not dusty enough to be collisionally decaying as a whole (but then, neither is our own system, for which $t_{\rm dd} \sim 10^6$ Gyr, 10^7 times longer than $t_{\rm dd}$ of β Pic, based either on the mass loss rate of ~ 10 tons s^{-1} from the meteoritic complex or on $\tau_m \sim 10^{-7}$, describing the zodiacal light disk).

5. THE ISM SANDBLASTING OF THE β PIC DISK

The purpose of this section, in which we consider the sandblasting by ISM occurring in the outer disk regions, is twofold. Using the results of §§ 3 and 4 for a comparison of externally and internally produced dust area and mass, we show quantitatively that ISM is unimportant for the overall existence and survival of the disk around an A-type star. Secondly, we propose that in spite of this, ISM sandblasting may have more subtle, but observable, effects. In particular, the directed streaming of ISM can cause some non-axisymmetry in the dust distribution outside of the avoidance radius that may be observable.

The dust production in ISM-disk interaction depends on the incoming flux of the ISM particles, in addition to the kinematics of the ISM grains (§ 3.2). The spatial density of the ISM dust is subject to large variations. During their main-sequence lifetime, Vega stars encounter many H I and molecular clouds, and reside inside them $\sim 3\%$ of the time (LG; Stern 1990). The rest of the time stars spend in warm and hot gas, which has little or no dust and so a less erosive action. It is not clear how many, if any, dust clouds β Pic has encountered since emerging from its natal ISM complex (could it possibly have been the Oph-Sco-Cen complex?), because the estimated time between encounters (~ 40 Myr for atomic and ~ 400 Myr for molecular clouds; Binney & Tremaine 1987) is comparable to this star's likely age. Therefore, the concept of erosion inside ISM clouds should be applied to β Pic with great caution. In any case, it is important to understand exactly what effects a dense ISM could cause.

The mean Galactic density of solid grains is $\bar{\rho} = 10^{-26}$ g cm^{-3} (assuming a dust-to-gas ratio of 10^{-2} and a mean

TABLE 3

MODELS OF DISK-ISM INTERACTION

No.	Notes	q	v_∞ (km s^{-1})	θ	$r_{\rm av}(0.1\ \mu{\rm m})$	$t_{\rm dd}$	$t_{\rm ISM}$	Fig.
1.....	...	1.7	8.6	45°	760 AU	67 Myr	34 Gyr	5 *top*
2.....	...	2	8.6	45°	760 AU	65 Myr	68 Gyr	...
3.....	$s_d = 3\ \mu$m	1.7	8.6	45°	760 AU	89 Myr	24 Gyr	...
4.....	Variable q	1.7–2.7	8.6	45°	760 AU	65Y Myr	270 Gyr	5 *bottom*
5.....	...	1.7	17.2	15°	190 AU	67 Myr	210 Myr	6 *top*
6.....	...	1.7	17.2	75°	190 AU	67 Myr	180 Myr	6 *bottom*
7.....	$\beta = 1.1$	2	8.6	45°	5 AU	65 Myr	1.1 Gyr	7
8.....	Big ISM dust	2	25	30°	90 AU	65 Myr	700 Gyr	7
9.....	α PsA disk	2.0	9.9	45°	880 AU	214 Gyr	3 Tyr	8

ISM density of 0.018 $M_\odot$ pc^{-3}, corresponding to a hydrogen density of ~ 1 cm^{-3}). Atomic H clouds have a 20 times higher density, but their filling factor is only $\phi = 0.025$ (Spitzer 1978). Molecular clouds fill merely $\phi \approx 0.002$ of the stellar disk with density between $10^3\bar{\rho}$ and $10^6\bar{\rho}$. The time-average erosive action of molecular and atomic clouds may be comparable (Stern 1990). Since it is more likely that β Pic and its A-type analogs entered atomic rather than molecular clouds in their relatively short lifetimes, we have chosen $\rho_{\rm dust} = 4.4 \times 10^{-25}$ g cm^{-3} as a characteristic density of solids in ISM, a value obtained by assuming a mean molecular weight of the gas as 1.3, and an H density of 20 cm^{-3} in standard atomic clouds. We should bear in mind that enhancements of $\rho_{\rm dust}$ by factors of up to 10^2–10^3 normally occur in molecular clouds, which will proportionally increase the erosion rates. On the other hand, the Sun (with its heliosphere) currently resides in a medium with a density of only $\sim 10^{-1}\bar{\rho}$.

5.1. *Description of the Model*

We modeled the β Pic disk as a flat, axisymmetric disk with surface density given by equation (7), extending from the star to an outer radius equal to 10^3 AU. The disk was bombarded at an angle θ to its plane by ISM grains with a size distribution given by equation (6) (20 size bins from 0.01 to 1 μm were typically used), uniform density $\rho_{\rm dust}$, and relative velocity v_∞. Although trajectories of dust can be expressed analytically, given the inclined disk geometry we found it easier to determine the velocity and density field of ISM grains crossing the disk midplane by numerically integrating their simple equations of motion (§ 3.1). The initial positions of ISM (projectile) particles were generated on an equidistant mesh of 64 by 64 points at a distance $\sim 10^4$ AU from the star. The projectiles, each representing the motion of a large number of actual ISM grains flowing per unit time through their respective initial-condition mesh element, were followed until they intersected the disk or passed it without collision.

At the moment of intersection, the probability of collision and the velocity components of the disk dust grains (targets) were generated, taking into account oblique passage through the disk and the collisional cross section of each projectile-target pair. The velocity field of targets in the disk is non–uniquely defined because of the considerable velocity dispersion, $\sigma = \beta_d/(1 - \beta_d)^{1/2} v_{\rm K}$, arising from their eccentric in-plane epicyclic motions and smaller vertical motions with respect to circular orbits (added by a random generator). Since the ISM and disk velocities are often of the same magnitude, the relative orientation as well as the speed of the targets' and projectiles' motion is very important. For each projectile, we numerically averaged results over time (13 epicycle phases of target). The models had sufficient resolution in all the variables to yield a reliable mean result.

The collisional outcome of each target-projectile collision was found by computing the specific energy ϵ released in the collision per unit target mass. The collision is considered to lead to catastrophic fragmentation and subsequent radiative blowout of debris if $\epsilon > Q^*$, were Q^* is the fragmentation strength of the silicate grain, $Q^* \sim 10^7$ ergs g^{-1} under typical laboratory conditions with centimeter-sized targets and impact speeds of $v \sim 0.8$ km s^{-1} (Gault & Wedekind 1969; Gault 1973; Davis & Ryan 1990; Fujiwara, Kamimoto, & Tsukamoto 1977; Fujiwara et al. 1989). A correction to account for the larger impact strength of microscopic targets and dependence on the rate of strain was applied in the form of the following weak power-law scaling (cf. Davis & Ryan 1990; Housen, Schmidt, & Holsapple 1991; Holsapple 1993):

$$Q^* = 10^7 (v/0.8 \text{ km s}^{-1})^{1/4} (s_d/10 \text{ cm})^{-1/4} \text{ ergs s}^{-1} . \quad (15)$$

According to this equation, β Pic grains with $s_d = 4$ μm under impact speeds on the order of 10 km s^{-1} have strength $Q^* \approx 2 \times 10^8$ ergs g^{-1}. Such a grain impacted by a typical ISM grain with $s = 0.1$ μm is not completely disrupted (shattered) unless $v \gtrsim 40$ km s^{-1}. At a smaller speed, $v = 9$ km s^{-1}, characteristic of ISM–β Pic relative motion, very large ISM grains, with $s > 0.35$ μm, are required for shattering.

The collision was classified as a cratering event and a correspondingly smaller mass of debris, equal to $\Delta m = \alpha m v^2/2$, was recorded for $\epsilon < Q^*$, where m denotes the projectile mass. We adopted a cratering coefficient $\alpha = 4 \times 10^{-10}$ g erg^{-1} (cf. Marcus 1969; Dohnanyi 1969). Catastrophic and cratering losses were counted separately and later compared in each of the 100 radial bins uniformly spaced in r and 10 AU wide. We have also produced maps of the local disk erosion by ISM (§ 5.2.4).

5.2. *Results of Modeling*

We present in Table 3 the parameters and results of models that we have computed. Unless otherwise stated, the second column of the table uses the β Pic disk model described by equation (7) with constant q and $r_m = 60$ AU, and dust with mean size $s_d = 4$ μm. Empirical size distribution (§ 3.2) of the ISM and the spatial density, $\rho_{\rm dust}$, of dust in atomic H I clouds were assumed; v_∞ and the flow angle θ were varied. The two main results of these calculations are the timescales $t_{\rm dd}$ and $t_{\rm ISM}$, the second given by equation (14) with $\dot{M}_{\rm dust}$ interpreted as being due to ISM.

5.2.1. *Models of β Pic*

Model 1 presents our standard choice of parameters: a β Pic disk with outer power-law profile $\tau \sim r^{-1.7}$, bombarded by ISM streaming at a 45° angle with $v_\infty = 8.6$ km s^{-1}. As already noted, the avoidance radius for the typical 0.1 μm ISM grains is $r_{0.1} = 580$ AU at that speed, and the depletion timescale, assuming a disk of 120 $M_{\rm E}$, is $t_{\rm dd} = 67$ Myr in this case. In contrast, the analogous destruction time for the total (erosive + shattering) effect of ISM sandblasting is very long, $t_{\rm ISM} = 34$ Gyr. This result is a direct consequence of the substantial avoidance zone surrounding β Pic. Figure 5 (*top panel*) shows the radial distribution of the dust destruction rate in model 1. Cratering and shattering processes are most effective at large distances and very ineffective inside the radius $r_{0.1}$ (which is, of course, penetrable for large grains). On the other hand, the internal dust grinding rate peaks inside a much smaller radius, on the order of $r_m = 60$ AU, and dominates the overall dust production by a factor of 10^3.

Model 2 has a somewhat different disk density profile, described by $q = 2$, that does not lead to very different results. Model 3, with radius $s_d = 3$ μm, smaller than in other models, is also similar in results to model 1. Somewhat larger differences are seen between models 1 and 4, the latter having a steeper outer profile, which was generated by using equation (7) with a radius-dependent exponent q, growing linearly from 1.7 to 2.7 between $r = 100$ AU and

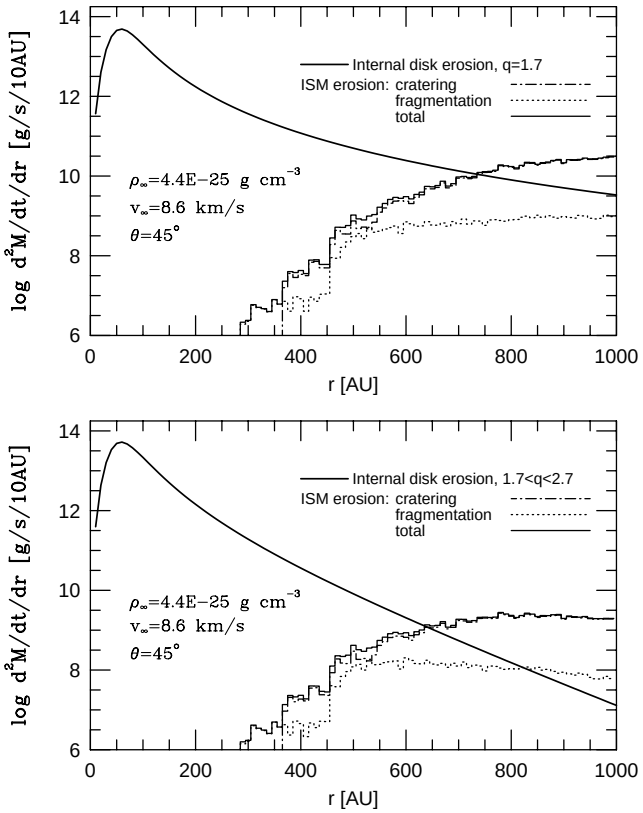

FIG. 5.—*Top*: Mass-loss rate from the β Pic disk per 10 AU radial interval. The overplotted standard model parameters (No. 1, Table 3) correspond to the passage of β Pic through a typical atomic H cloud. *Bottom*: The same as the top panel, but for a modified density distribution (see text and No. 4, Table 3), which truncates faster at large radii.

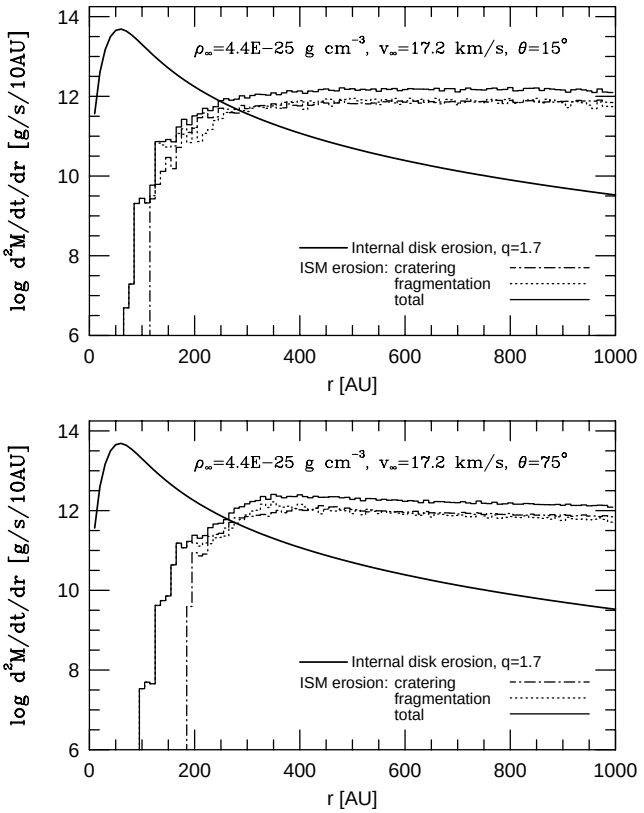

FIG. 6.—Comparison of two ISM–β Pic disk interaction models (No. 5 and 6 in Table 3) with double the standard inflow velocity of Fig. 5 and two disk inclinations, one close to edge-on (*top*; 15°) and one close to pole-on (*bottom*; 70°).

1000 AU. While the outer disk density is not yet known in detail, a profile of this type is fully admissible, and even more likely in view of the steepening power law of scattered light profile observed in β Pic (Golimowski et al. 1993 and references therein). The differences between the truncated and single power-law models can be seen in the bottom panel of Figure 5. ISM-disk interaction generates locally more debris than disk-disk processes in the outer region of the truncated model, but much less dust in absolute terms.

The top and bottom panels of Figure 6 present the dust production in a fast encounter ($v_\infty = 17.2$ km s^{-1}) of the β Pic disk with ISM medium streaming at angles 15° and 75°, respectively, to the disk plane (models 5 and 6). At this velocity, two times higher than the expected value for β Pic, a significant fraction of the ISM grain spectrum can shatter the average disk grain in one strike, such that grain cratering and catastrophic fragmentation produce comparable amounts of debris. There are only subtle differences between the results of models 5 and 6, especially outside the inner region dominated by the specific geometry of dust flow (§ 3.1). This is expected, since as long as impact velocities remain close to v_∞, erosion of any given disk grain is independent of θ.

Interestingly, however large the overall dominance factor of internal dust collisions over ISM-disk processes might be (it ranges from 3 to 10^4 in our β Pic models in Table 3), the ISM is always locally dominant in the outer disk region at $r \geq r_{\rm ISM}$, where $r_{\rm ISM}$ ranges between 250 AU for fast encounters (models 5 and 6, and the artificial $\beta = 1.1$ model 7) to 650–750 AU in standard cases (models 1–4). This suggests the possibility of observable distortion of the outer disk regions caused by ISM (see § 5.2.4 below).

The radius $r_{\rm ISM}$ depends on ρ_∞. It is easy to rescale the results of any model to ISM densities smaller or larger than our choice, corresponding to an atomic H cloud with $n_{\rm H} = 2$ cm^{-3}, by shifting the histograms along the vertical axis ($d^2M/dt/dr \propto \rho_\infty$). It is straightforward to see that the average Galactic density of grains, about 40 times smaller than $\rho_\infty = 4.4 \times 10^{-25}$ g cm^{-3}, moving at 8.6 km s^{-1} or less toward β Pic, could not compete with disk processes anywhere in the disk except perhaps at its barely visible outer edge ($r_{\rm ISM} \sim 10^3$ AU). This suggests that at present β Pic is totally immune to the erosive action of ISM.

What conditions must be met to lead us to an opposite conclusion, i.e., that ISM sandblasting is important, maybe even crucial for disk evolution? Increasing the ISM density by the factor of 1000 above that of atomic clouds (which might simulate molecular cloud environment) would decrease the ISM-dominance radius from $r_{\rm ISM} = 760$ AU to 400 AU (Fig. 5, *top*) and cause a larger mass loss through ISM than through disk collisions. Still, the effect would only be felt inside the molecular cloud, and it would vanish within 10^4 yr after the star leaves the cloud. The time-average effect of such encounters would not be dominant, due to the small filling factor of molecular clouds. And finally, the effect of ISM in our models is always distributed over a large area of a low-density disk region. Very few observations reach those outer disk parts, most concentrating on the region $r \lesssim 200$ AU, where the ISM dust is com-

pletely forbidden to enter independent of its spatial density (unless an ad hoc, high v_∞ is assumed).

In model 7 we depart from realistic conditions connected with the physical nature and optical properties of ISM dust grains to find out to what extent our results are due to stellar radiation pressure. We artificially (nearly) balance radiation against gravity by setting $\beta = 1.1$ for all the grains, while keeping their size distribution as in models 1–6. A qualitatively similar reduction of β could be obtained by replacing the A5 star by a star of type later than G. In this way, the avoidance radius is reduced almost to zero, as shown in Table 3 and Figure 7. The local dust destruction rate at the maximum disk density around $r = 50$ AU increases to $\sim 10^{-2}$ of the internal disk erosion, but neither it nor the total dust destruction becomes ISM dominated. This shows that very unusual conditions involving high velocities and high ISM densities would be necessary to exceed the intense internal dust processing in β Pic. The β Pic disk seems to be doubly protected from the influence of ISM by the stellar radiation pressure and by its high density. Other disks may rely more on the radiation pressure for their protection.

5.2.2. *Large ISM Grains*

Model 8 studies the effects of very large, atypical ISM grains, such as those streaming at $v_\infty \sim 26$ km s^{-1} through the solar system at a density of $\sim 1.6 \times 10^{-27}$ g cm^{-3}, as measured by *Ulysses* (Grün et al. 1993, 1994). The grains measure on average $s \sim 0.4$ μm, and are much more massive ($m \sim 3 \times 10^{-13}$ g) than typical ISM grains. Their presence in the region of Jupiter (and simultaneous absence at a 700 times smaller density around Earth) demonstrates that complicated dust-heliosphere interactions involving magnetic forces may deflect and keep out small ISM grains, while only the atypical grains are admitted and focused around the sun. The filtering role of the magnetic field is taken over by a larger radiation pressure in β Pic, but the presence of a similar background of fast, large ISM grains may be expected around the star as well. We model such grains by preserving the shape of the distribution dN/ds from equation (6) and shifting it to 10 times larger radii (even somewhat larger than *Ulysses* probe measurements, to bring out possible effects). Figure 7 includes the results of model 8. Despite the fact that the ISM grains are now able to catastrophically shatter disk grains (unlike other models, in ours cratering is negligible and thus is not shown on the plot), the local and total sandblasting effect of large ISM grains is very small because of their small number density in the ISM.

5.2.3. *The α PsA System*

Finally, model 9 is devoted to the system of α PsA, the second strongest example of Vega phenomenon among disk systems (Backman & Paresce 1993), with about a 50 times smaller dust-covering factor than β Pic. Based on its infrared excess spectrum, we adopt $r_m = 90$ AU for this system, and obtain a normalization factor $\tau_m = 0.96 \times 10^{-4}$. The mean dust-dust collision time is on the order of 1 Myr. Figure 8 presents the resulting mass loss rates. As anticipated in § 4.3, the timescale for planetary system depletion by dust collisions turns out to be exceedingly long ($t_{dd} =$ 214 Gyr). The intense radiation pressure excludes 0.1 μm grains from most of the model disk ($r_{0.1} = 880$ AU), entailing an even longer ISM erosion time, $t_{ISM} \sim 10 t_{dd}$. The smaller dust-covering factor of more typical Vega-type systems is not by itself a guarantee of the dominance of ISM erosion.

5.2.4. *Asymmetries in ISM Sandblasting*

The low-density dust at $r > r_{ISM}$ is destroyed primarily by the ISM. Submicron-sized debris produced by the ISM leave the disk generally from the same quadrant in which they were created, thus carrying information about any asymmetries in disk erosion. There are two reasons for the lack of axisymmetry in interactions with ISM. First and foremost, unless $\theta \approx 90°$, the overlapping paraboloidal walls of grain-free wakes create a sickle-shaped area of intersection with disk, subject to intense bombardment. We illustrate its shape in Figure 9, based on model 1. (Only the ISM contribution to disk erosion is presented.) The quantity shown is $\dot{M}$ per unit disk area, or $\dot{\Sigma}$.

Figure 9 also shows clearly the second (up-down) asymmetry, caused by the rotation of the disk. Much more erosion of the disk will occur on that arm of the sickle where the mean disk rotation is directed oppositely to ISM

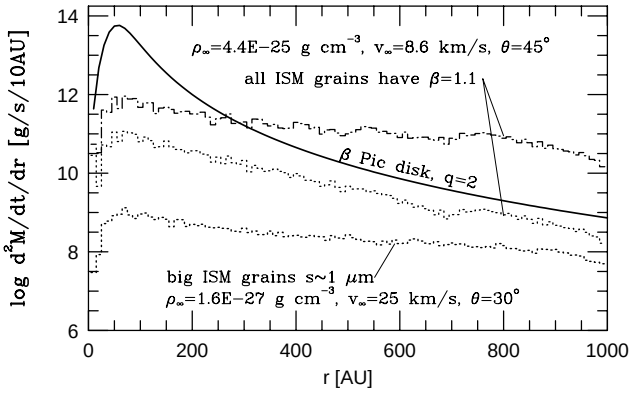

FIG. 7.—Results of the interaction of the β Pic disk (with $q = 2$) with two nonstandard collections of bombarding grains. Meanings of the lines are the same as in Figs. 5 and 6. Two upper curves present the ISM grain size distribution with radiation pressure artificially reset to 1.1 times gravity (No. 7 from Table 3). The lower curve corresponds to No. 8 from Table 3, simulating the rarefied population of large ISM grains that have been observed in the solar system.

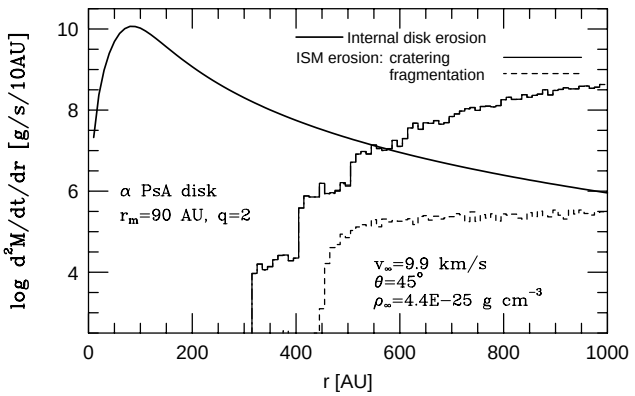

FIG. 8.—A model of the β Pic disk (No. 9, Table 3) with parameters modified to describe the disk around α PsA, interacting with the dust of a typical atomic H cloud.

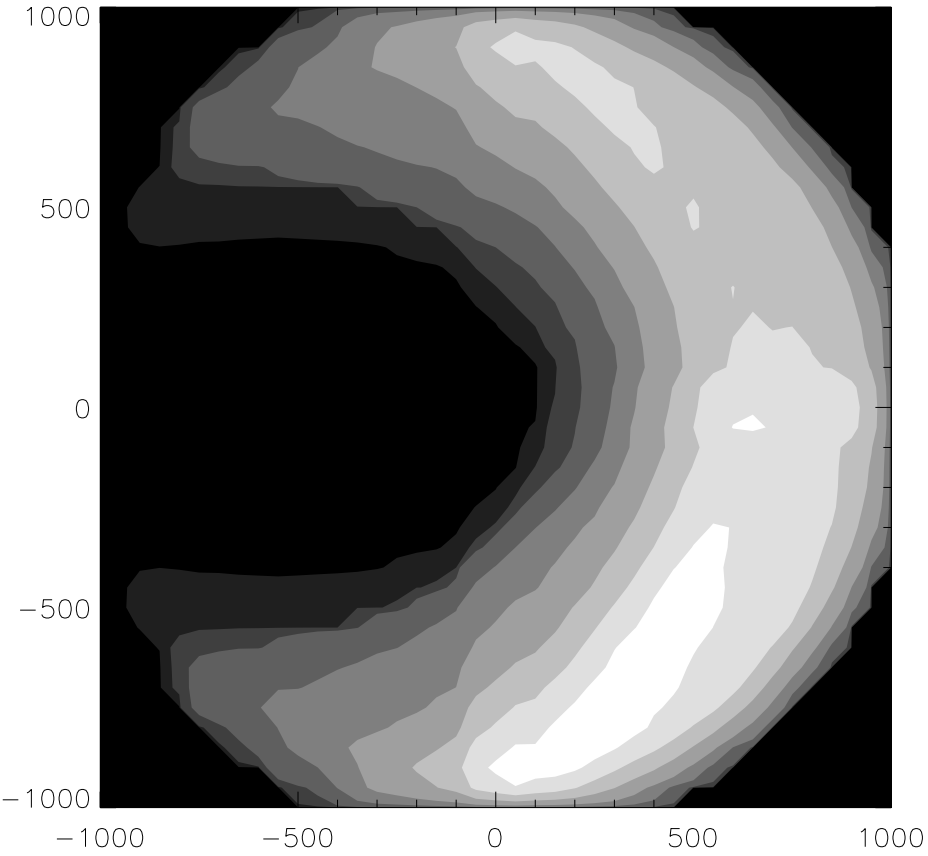

FIG. 9.—Pole-on view of the dust destruction rate by ISM in β Pic disk (No. 1, Table 3). Dust enters from the right at an angle $\theta = 45°$ to the disk plane. Distances on axes are given in AU, and the star lies at the origin. Isocontours of $d\Sigma/dt$ in units of g s^{-1} AU^{-2} are (from the largest, bounding white area): 1.6×10^6, 9.6×10^5, 4.8×10^5, 1.6×10^5, 4×10^4, 4×10^3, 400, and 40. The pronounced left-right asymmetry is caused by $\theta < 90°$, while the up-down asymmetry is caused by disk rotation.

streaming, effectively increasing v_∞ by about $v_c(r)$. In model 1 this asymmetry reaches on the average a factor of 2 (up to 4 at selected radii) when comparing dust production below and above the horizontal axis, counterrotating vs. corotating with the ISM flow. Similar results were obtained in other models, including those with other inclination angles θ. In general, however, the left-right asymmetry is much larger than the up-down one.

While ISM-disk interaction can lead to the markedly nonsymmetric planar outflow of debris, we do not expect substantial vertical motion or asymmetries of debris away from the disk plane because of the large mass difference between targets and projectiles, which causes the bulk of the debris to follow the nearly planar motion of the center of mass of each pair of colliding particles.

It would be interesting to calculate the density, optical thickness, and color of β meteoroids leaving the disk and compare their projections onto the sky with images of β Pic. This task is beyond the scope of the present paper. (For one thing, optical thickness of the outflowing grains produced by internal disk processing must first be reliably established.) This issue deserves attention because of the possible connection with the observed outer disk asymmetries (Kalas & Jewitt 1995). Our results show that in atomic clouds, the total dust destruction rate due to ISM is subdominant. Therefore, if the optical thickness of β meteoroids is at all observable, disk asymmetries due to ISM-disk interaction can only be present in the outermost, most difficult to observe disk regions at $r \gtrsim r_{\rm ISM}$. Conversely, a firm observational exclusion of color differences between the NE and SW extensions would eliminate the ISM sandblasting.

6. DISCUSSION AND CONCLUSIONS

6.1. *Critique of "Environmental" Interpretations of Vega Phenomenon*

In § 2 we confronted on their own ground the two current theories relating the dust contents of at least some Vega-type systems to their interaction with ISM. Much space has been devoted to the reevaluation of the kinematics of A-type stars, which formed the basis for WMW's proposal of correlated spatial motions for their sample of prominent Vega systems that were supposed to lead them (~ 10 Myr back in time) to the Lup-Cen complex. We have found little evidence that kinematical streaming is what distinguishes them from normal A-type stars. While it appears quite possible that some of the five selected Vega stars did intersect Lup-Cen clouds, an even larger number of control stars could also have done so.

We feel that the alternative theory of Lissauer & Griffith (1989), that ISM sandblasting occurs with widely varying efficiency due to different v_∞ (relative encounter velocity), is also open to criticism, because the authors identify v_∞ with stellar velocity, v_* (in LSR), while we take into account substantial ISM velocity, $v_{\rm ISM}$, as well. If, as the authors propose, the conspicuousness of β Pic arises from the lack

of ISM erosion, then we would expect to find a significantly lower v_∞ for that star compared to others. However, from equation (5) and v_* from Table 1 we see that all prominent Vega systems have $v_\infty \sim 10$ km s^{-1}; β Pic does not enjoy any privileged status. Therefore, we cannot confirm LG's conclusion resting only on the stellar velocity v_*.

In § 3 we have outlined the basic physical reason for our assertion that ISM sandblasting has little to do with whether or not a given star (especially Vega, Fomalhaut, β Pic, and other A-type stars) has a dense dust disk. We draw attention to the fact that ISM dust contains dark, absorbing components (e.g., Mathis 1996) that produce large radiation pressure coefficients in the radiation field of an early-to-intermediate type star. The dust avoids being within one or two times the avoidance radius (eq. [1]) from the star, depending on initial inclination. In practice, the avoidance radii around A-type stars for grains dominating in ISM clouds are from several to tens of times larger than radii of maximum dust density (which are routinely found from spectral modeling to be on the order of $r_m \sim 50$–150 AU, and confirmed directly to be ~ 50 AU in β Pic).

The lack of spatial overlap relegates the effects of ISM erosion, if any, to the outer disk parts, beyond the most essential, dense inner regions. In § 5, we have presented detailed calculations of the ISM sandblasting of β Pic and α PsA disks (assuming that the latter is structured similarly to the former), and find that passage through a standard atomic hydrogen cloud can lead to a local dominance of ISM erosion over internal erosion at the very outskirts of the disks. Nevertheless, most erosion will always occur in the shielded inner regions. The overall evolution of the disk material should not depend on the environment.

6.2. *What Produces the Dust Around Main-Sequence Stars?*

Having concluded that the dust disks are not created (or destroyed) by their environment, we must ask, What is their true origin and why do they differ so much in appearance? In fact, more than a decade after its discovery and in apparent contradiction to the ubiquity of β Pic-type IR excesses among normal stars, β Pic remains at present the only Vega-type star with a well-resolved disk seen in the scattered light (with the one possible exception of BD +31 643; Kalas & Jewitt 1997), although thermal images of some other objects show elongated silhouettes of inclined disks. Some light can be shed on this question by studying the internal dust processing, as we have done in § 4. We have outlined the somewhat unfamiliar dynamics of radiation-pressure affected, gas-poor disks (in which gas drag is unimportant on collisional timescales; β Pic is very gas-poor except perhaps for the inner ~ 1 AU circle).

The observed dust grains, though not the whole disk, are ephemeral. Born in collisions, or released from evaporating bodies,[5] the typical disk grains in the moment of detachment from a larger parent body feel the force of gravity reduced by radiation pressure. (For typical grains we understand the area-dominating grains at the lower cutoff or knee in the otherwise steep size spectrum, such as $dN \sim s^{-3.5}ds$; the cutoff size is the blowout size for which $\beta = 1$.) The radiation pressure on typical grains is at least comparable to gravity. Many grains do not survive in stable orbits but are promptly ejected from the system, in a way similar to the escaping β meteoroids and tails of comets in the solar system. We are mainly observing the remaining α meteoroids that survive in the disk on elliptic orbits of widely distributed, noticeable eccentricity. Our estimates have shown that substantial eccentricities are present, with the mean around $e_d \approx \frac{1}{3}$. This implies vigorous radial and azimuthal velocity dispersion, several times larger than the vertical velocity dispersion following from the observed disk thickness in β Pic. Particle fluxes, capability for cratering (proportional to the square of velocity), and other quantities are thus larger than previously thought.

A heuristic model of dust-dust collisions, neglecting the detailed treatment of the size spectrum of disk particles, results in dust residence times as short as 10^4 yr at the maximum density radius of ~ 60 AU from β Pic, and a large overall dust destruction rate of 2 Earth masses per Myr. We stress that even the standard evaluation of collisional timescales using the vertical rather than planar velocity dispersion would yield destruction times only a few times longer, leaving our main conclusions unaffected. (More detailed treatments, to be described in forthcoming publications, lead to similar results.) Unless the β Pic disk is short-lived or very nonstationary, or its circumstellar material much more massive than following from cosmochemical constraints and observations of protostellar disks (neither alternative being likely), the age of the disk must be $\lesssim 10^2$ Myr. The star may be surrounded by an analogue of the Kuiper belt (e.g., Weissman 1995; Backman, Dasgupta, & Stencel 1995; Artymowicz 1997). Since β Pic is on the main sequence, the system's likely age ranges from 20 Myr(?) to about 100 Myr (cf. Crifo et al. 1997). In contrast, most Vega-type stars are older. They are also much less dusty, and the collisional cascade does not drive their overall evolution, although it does remove and regenerate dust many times over the star's age (e.g., on a timescale of ~ 1 Myr in α PsA). One of the most important factors in the prominent position of β Pic among its kin may thus be its relatively young age, suggesting that β Pic may now be actively clearing itself of solid debris from a recent formation epoch. The present high dust removal rate and high dust content must decline markedly within the next $t_{\rm dd} \sim 65$ Myr.

If great dustiness is a sign of young age, it is also a somewhat ambiguous indicator. There may not be a unique dustiness vs. time relation for all systems. The rate at which β Pic-type systems become less dusty may depend on many factors; for instance, on the rapidity of planet formation. Through various means, including the study of dust perturbed dynamically by planets, we hope to eventually determine such factors.

We thank D. Backman, P. Kalas, and G. Gahm for informative discussions, and R. Bohlin for sharing the recalibrated *IUE* stellar fluxes. We utilized the SIMBAD database available from CDS in Strasburg. A. Vidal-Madjar kindly supplied the preprints by Crifo et al. (1997) and Vidal-Madjar (1997), which allowed us to use an updated distance and luminosity of β Pic in our models. P. Kalas and an anonymous referee helped improve the presentation. P. A. acknowledges the support of the Visitor Program at STScI. This research was partly supported by NFR (Swedish Natural Science Research Council).

[5] A less likely possibility, in view of the large quantity of dust required; cf., however, Lecavelier des Etang, Vidal-Madjar, & Ferlet (1996), who concentrate on the qualitative aspects. The choice between collisions of meteoroids and evaporation of comets does not weaken the following argument; the cometary option would actually strengthen it by adding finite parent-body eccentricity.

REFERENCES

Aitken, D. K., et al. 1993, MNRAS, 265, L41
Artymowicz, P. 1988, ApJ, 335, L79
———. 1994a, in Dust Disks and Planet Formation, ed. R. Ferlet & A. Vidal-Madjar (Gif sur Yvette: Editions Frontieres), 47
———. 1994b, in Dust Disks and Planet Formation, ed. R. Ferlet & A. Vidal-Madjar (Gif sur Yvette: Editions Frontieres), 335
———. 1996, in The Role of Dust in the Formation of Stars, ed. H. U. Käufl & R. Siebenmorgen (Berlin: Springer), 137
———. 1997, Annu. Rev. Earth Planet. Sci., 25, 175
Artymowicz, P., Burrows, C., & Paresce, F. 1989, ApJ, 337, 494
Aumann, H. H., et al. 1984, ApJ, 278, L23
Aumann, H. H., & Good, J. C. 1990, ApJ, 350, 408
Backman, D. E., Dasgupta, A., & Stencel, R. E. 1995, ApJ, 450, L35
Backman, D. E., Gillett, F. C., & Witteborn, F. C. 1992, ApJ, 385, 670
Backman, D. E., & Paresce, F. 1993, in Protostars and Planets III, ed. E. H. Levy, J. I. Lunine, & M. S. Matthews (Tuscon: Univ. Arizona Press), 1253
Beust, H., & Morbidelli, A. 1996, Icarus, 120, 358
Beust, H., Vidal-Madjar, A., Ferlet, R., & Lagrange-Henri, A. M. 1994, ApS&S, 212, 147
Binney, J., & Tremaine, S. 1987, Galactic Dynamics (San Francisco: Freeman)
Bohren, C. F., & Huffman, D. R. 1983, Absorption and Scattering of Light by Small Particles (New York: Wiley)
Burns, J. A., Lamy, P. L., & Soter, S. 1979, Icarus, 40, 1
Burrows, C., et al. 1995, BAAS, 187, 32.05
Crifo, F., Vidal-Madjar, A., Lallement, R., Ferlet, R., & Gerbaldi, M. 1997, A&A, in press
Davis, D. R., & Ryan, E. 1990, Icarus, 83, 156
Dohnanyi, J. S. 1969, J. Geophys. Res., 74, 2531
Draine, B. T., & Lee, H. M. 1984, ApJ, 285, 89
Eggen, O. J. 1983, MNRAS, 204, 391
Fujiwara, A., et al. 1989, In Astroids II, ed. R. Binzel, T. Gehrels, & M. S. Matthews (Tucson: Univ. Arizona Press), 240
Fujiwara, A., Kamimoto, G., & Tsukamoto, A. 1977, Icarus, 31, 277
Gault, D. E. 1973, Icarus, 2, 121
Gault, D. E., & Wedekind, J. A. 1969, J. Geophys. Res., 74, 6780
Gliese, W. 1969, Veröffentlichungen des Astronomischen Rechen-Instituts Heidelberg No. 22, Catalogue of Nearby Stars (Karlsruhe: Braun)
Golimowski, D. A., Durrance, S. T., & Clampin, M. 1993, ApJ, 411, L41
Grün, E., et al. 1994, A&A, 286, 915
Grün, E., Zook, H. A., Fechting, H., & Giese, R. H. 1985, Icarus, 62, 244
Grün, E., et al. 1993, Nature, 362, 428
Holsapple, K. A. 1993, Annu. Rev. Earth Planet. Sci., 21, 333
Housen, K. R., Schmidt, R. M., & Holsapple, K. A. 1991, Icarus, 94, 180
Kalas, P., & Jewitt, D. 1995, AJ, 110, 794
———. 1997, Nature, 386, 52
Kim, S.-H., & Martin, P. G. 1995, ApJ, 444, 293
Kim, S.-H., & Martin, P. G. 1996, ApJ, 462, 296
Kim, S.-H., Martin, P. G., & Hendry, P. D. 1994, ApJ, 422, 164
Knacke, R. F., et al. 1993, ApJ, 418, 440
Lagage, P. O., & Pantin, E. 1994, Nature, 369, 628
Lagrange, A. M. 1995, Ap&SS, 223, 19
Lamy, P. L., Grün, E., & Perrin, J. M. 1987, A&A, 187, 767
Lazzaro, D., Sicardy, B., Roques, F., & Greenberg, R. 1994, Icarus, 108, 59
Lecavelier des Etang, A., et al. 1993, A&A, 274, 877
Lecavelier des Etang, A., Vidal-Madjar, A., & Ferlet, R. 1996, A&A, 307, 542
Leinert, C., Röser, S., & Buitrago, J. 1983, A&A, 118, 345
Lissauer, J. J., & Griffith, C. A. 1989, ApJ, 340, 468 (LG)
Marcus, A. H. 1969, Icarus, 11, 76
Mathis, J. S. 1996, ApJ, 472, 643
Mathis, J. S., Rumpl, W., & Nordsieck, K. H. 1977, ApJ, 449, 320
Mihalas, D., & Binney, J. 1981, Galactic Astronomy (San Francisco: Freeman)
Norman, C. A., & Paresce, F. 1989, in The Formation and Evolution of Planetary Systems, ed. H. Weaver & L. Danly (Cambridge: Cambridge Univ. Press), 151
Paresce, F. 1991, A&A, 247, L25
Paresce, F., & Artymowicz, P. 1989, in Structure and Dynamics of the ISM, ed. G. Tenorio-Tagle, M. Moles, & J. Melnick (Berlin: Springer), 221
Paresce, F., & Burrows, C. 1987, ApJ, 319, L23
Patten, B. M., & Willson, L. A. 1991, AJ, 102, 323
Roques, F., Scholl, H., Sicardy, B., & Smith, B. A. 1994, Icarus, 108, 37
Sicardy, B. 1994, in Asteroids, Comets, Meteoroids 1993, ed. A. Miliani, et al. (Dordrecht: Kluwer), 429
Smith, B. A., & Terrile, R. J. 1984, Science, 226, 1421
Spitzer, L. 1978, Physical Processes in the Interstellar Medium (New York: Wiley)
Stern, S. A. 1990, Icarus, 84, 447
van Altena, W. F., Lee, J. T., & Hoffleit, E. D. 1995, The General Catalogue of Trigonometric Stellar Parallaxes, Vol. I (New Haven: Yale Univ. Observatory)
Vidal-Madjar, A., Lecavelier, A., & Ferlet, R. 1997, Ap&SS, submitted
Walker, H. J., & Wolstencroft, R. D. 1988, PASP, 100, 1509
Weissman, P. R. 1995, ARA&A, 33, 327
Westin, T. 1985, A&AS, 60, 99
Whitmire, D. P., Matese, J. J., & Whitman, P. G. 1992, ApJ, 388, 190 (WMW)
Wolff, M. J., Clayton, G. C., Martin, P. G., & Schulte-Ladbeck, R. E. 1994, ApJ, 423, 412
Wolff, M. J., Clayton, G. C., & Meade, M. R. 1993, ApJ, 403, 722
Zuckerman, B., & Becklin, E. E. 1993, ApJ, 414, 793